Experimental determination of the diffusion coefficient in two-dimensions in ferrous sulphate gels using the finite element method.

C.Baldock [1], P. J.Harris [2], A.R.Piercy [3] and B.Healy [4]

[1] *Centre for Medical and Health Physics, Queensland University of Technology, Brisbane, Australia*
[2] *School of Computing and Mathematical Sciences, University of Brighton, United Kingdom*
[3] *School of Engineering, University of Brighton, United Kingdom*
[4] *Queensland Radium Institute, Mater Hospital, Brisbane, Australia*

Abstract

A novel two-dimensional finite element method for modelling the diffusion which occurs in Fricke or ferrous sulphate type radiation dosimetry gels is presented. In most of the previous work, the diffusion coefficient has been estimated using simple one-dimensional models. This work presents a two-dimensional model which enables the diffusion coefficient to be determined in a much wider range of experimental situations. The model includes the provision for the determination of a drift parameter. To demonstrate the technique comparative diffusion measurements between ferrous sulphate radiation dosimetry gels, with and without xylenol orange chelating agent and carbohydrate additives have been undertaken. Diffusion coefficients of 9.7±0.4, 13.3±0.6 and 9.5±0.8 10^{-3} cm^2h^{-1} were determined for ferrous sulphate radiation dosimetry gels with and without xylenol orange and with xylenol orange and sucrose additives respectively.

Introduction

Individuals have endeavoured to measure spatial absorbed radiation dose distributions over many years. In the 1950's methylene blue dye was used to determine radiation dose from colour changes in gels[1] and depth doses of X-rays and electrons in agar gels using spectrophotometry[2].

In 1984, it was proposed that nuclear magnetic resonance (NMR) relaxation measurements of particular irradiated materials could be used to determine absorbed dose of ionising radiation[3]. The first dosimeter to be investigated was the ferrous sulphate or Fricke dosimeter[4] In this radiation dosimetry system ionizing radiation causes ferrous (Fe^{2+}) ions to be converted to ferric ions (Fe^{3+}) through radiolysis of the aqueous system. Ferric ions exhibit a larger paramagnetic enhancement than ferrous ions and the magnetic resonance longitudinal (spin-lattice), R_1 and transverse (spin-spin), R_2 relaxation rates ($1/T_1$ and $1/T_2$ respectively) of the dosimeter are related to the concentration of Fe^{3+} produced, and hence to absorbed radiation dose[3]. It was found that changes in the relaxation properties of the irradiated dosimeters could also be measured using magnetic resonance imaging (MRI). Ferrous sulphate solutions were incorporated into a gel matrix in order to stabilize the irradiated MRI absorbed dose signature spatially. Longitudinal and transverse relaxation rate image 'maps' could then be used to quantify absorbed radiation dose distributions spatially.

Corresponding author: Clive Baldock Centre for Medical and Health Physics School of Physical Sciences Queensland University of Technology GPO Box 2434, Brisbane Q 4001 Australia E-mail: c.baldock@qut.edu.au
Received 19.06.01, Accepted 07.01.01

Since it was first shown that MRI may be used to measure absorbed dose distributions in ferrous sulphate gels many workers have subsequently investigated various aspects of this and other gel dosimetry systems. A major limitation in the application of ferrous sulphate gel dosimetry is the diffusion of ions in the dosimeter, resulting in an unstable absorbed dose distribution and subsequent error in the spatial dose measurement. This limitation has been investigated by a number of authors[5-14]. The effects of using chelating agents in reducing the diffusion of ions in ferrous sulphate gels has also been investigated[12,13].

Table 1 summarises some diffusion measurements by researchers in ferrous sulphate based dosimetry gels.

A number of previous studies on diffusion of ions in dosimetry gels have acquired relaxation measurements and subsequently calculated relaxation images. However, this approach does potentially require prolonged imaging times. In the current study, changes in image signal intensity have been investigated similar to other authors in their studies in gel dosimetry adopted this approach[12,15-17].

In a previous communication the development of a finite-element method to model the diffusion problem in Fricke based radiation dosimetry gels (Harris *et al* 1996) was reported. The method was used to measure the diffusion coefficient at different temperatures[9,10,18]. It was stated that the method could be extended to two or three-dimensions unlike other published methods that are essentially one-dimensional. An extended two-dimensional method along with the associated mathematical formulation is presented here. Since the determination of the diffusion coefficients is often complicated by signal drift, the present method incorporates

Reference	Diffusion Coefficient (10^{-3} cm^2h^{-1})	Gel Type & Concentration (%)	Other Constituents (mM)	Temperature (°C)
Schulz (1990)	18.3±1.4	A 1	S 12.5, Fe3+ 1	-
Schulz (1990)	15.8±1.1	A 1	S 25, Fe3+ 1	-
Olsson (1992)	19.1±1.0	A 1.5	S 50, Fe2+ 1	25
Gambarini (1994)	10.9±1.6*	A 1	S 50, Fe2+ 1, NaCl 1	15-17.5
Balcom (1995)	9.7±1.1	A 1	S 30, Fe2+ 1	22
Balcom (1995)	11.9±1.8	A 1	S 30, Fe2+ 1	22
Baldock (1995)	12.5±1.1	Agar	S 50, Fe2+ 1, NaCl 1	5
Baldock (1995)	21.3±0.5	Agar	S 50, Fe2+ 1, NaCl 1	24
Rae (1996)	8.2±0.1	G 4	S 26, Fe2+ 0.2, BE 5	10
Rae (1996)	9.1±0.1	G 4	S 26, Fe2+ 0.2, BE 5, Fo 70	20
Rae (1996)	10.4±0.1	G 4	S 26, Fe2+ 0.2, BE 5, P 0.6	10
Rae (1996)	4.4±0.1	G 4	S 26, Fe2+ 0.2, BE 5, P 0.6	10
Rae (1996)	0.7±0.1	G 8	S 26, Fe2+ 0.2, BE 5, Fo 46	20
Rae (1996)	1.0±0.1	G 8	S 26, Fe2+ 0.2, BE 5, Fo 46, P 0.6	20
Rae (1996)	4.4±0.1	G 4	S 26, Fe2+ 0.2, BE 5, XO 0.2	10
Rae (1996)	6.5±0.1	G 4	S 26, Fe2+ 0.2, BE 5, BD 0.6	10
Rae (1996)	6.1±0.1	G 4	S 26, Fe2+ 0.2, BE 5, Fo 46, XO 0.2	20
Rae (1996)	6.3±0.1	G 4	S 26, Fe2+ 0.2, BE 5, AC 0.6	20
Rae (1996)	8.3±0.1	G 4	S 26, Fe2+ 0.2, BE 5	10
Kron (1997)	14±3	A 1.5	S 50, Fe2+ 0.5	22
Kron (1997)	20±5	A 1.5	S 100, Fe2+ 0.5	22
Kron (1997)	22	A 1.5	S 200, Fe2+ 0.5	22
Kron (1997)	11	A 1.5	S 50, XO 0.25	22
Kron (1997)	5±1	G 10	S 50 & 100, Fe2+ 0.5	22
Kron (1997)	9	A 1.5, G 3	S 50, Fe2+ 0.5	22
Kron (1997)	9	A 1, G2	S 200, Fe2+ 0.5, XO 0.2	22
Kron (1997)	3±1	A 1.5, G 3	S 50 & 100, Fe2+ 0.5, XO 0.1 & 0.25	22
Pedersen (1997)	14.6±0.1	G	S 50, Fe2+1.5, XO 1.5	-
Pedersen (1997)	8.1±0.1	G	S 50, Fe2+1.5, XO 1.5	-
Pedersen (1997)	8.2±0.1	G + BA	S 50, Fe2+1.5, XO 1.5, BE 5.0	-
Pedersen (1997)	17.8±0.2	A 1.5	S 50, Fe2+1.5, XO 1.5	-
Pedersen (1997)	16.3±0.2	A 3	S 50, Fe2+1.5, XO 1.5	-
Chu (2000)	1.4	PVA 20	S 50, Fe2+ 0.4, XO 0.4	20

Table 1. *CSummary of diffusion measurements in the literature. A = agarose, Agar = agar, g = gelatine, PVA = polyvinyl alcohol, S = H_2SO_4, XO = xylenol orange, BE = benzoic acid, Fo = formaldehyde, P = phenanthroline, AC = acetylacetone, BD = bathophenanthroline disulfonic acid • Diffusion coefficient calculated in Rae1996.*

provision for modelling this effect by including a drift parameter in the governing equations. The diffusion coefficient and drift parameter are determined from experimental data by finding the values which minimise the difference between the distribution of the concentrations obtained experimentally and distribution of the concentrations obtained theoretically using the finite element method. This minimisation process could be carried out using any standard technique appropriate for solving an unconstrained optimisation problem. To demonstrate the technique comparative diffusion measurements between ferrous sulphate gels with and without the xylenol orange chelating agent have been undertaken. It was previously suggested that carbohydrate additives might improve ferrous sulphate gel sensitivity[19]. Diffusion measurements with sucrose additive were also undertaken as part of this study.

It has been stated that the finite element method requires a mathematical framework that is not readily available and that potential problems existed in specifying initial boundary conditions[14]. This is clearly not the case as the finite element method utilises mathematical resources available in most university libraries along with software available as part of numerous packages.

The technique presented here is a generic method for the determination of the diffusion coefficient which may be used for solving other diffusion problems not associated with either MRI or radiation sensitive gels.

Methods

Gel Manufacture

For this study three different formulations of ferrous

sulphate agarose gels were manufactured. Preparation of the dosimetry gels was according to the method of Zahmatkesh[20].

The first formulation of gel to be manufactured was ferrous sulphate agarose gel with xylenol orange chelating agent (FAX).

The FAX gel was manufactured using two glass beakers. One glass beaker contained 125 ml of singly distilled water, 25 mM of sulphuric acid (H_2SO_4), 0.4 mM ferrous ammonium sulphate ($Fe(NH_4)_2(SO_4)_2$) and 0.2 mM of xylenol orange chelating agent. It had previously been shown that for reproducible results the order that the ingredients were added was important[20]. The ferrous sulphate had to be dissolved before adding the xylenol orange dye. The mixture was stirred until a uniform solution was obtained. In the other glass beaker, 1% by weight of agarose powder was added to another 125 ml of distilled water and stirred until mixed thoroughly. The agarose glass beaker was heated to boiling in a microwave oven until a clear liquid was obtained. The heating time depended on the volume of the gel. For a 250 ml total volume this heating time was about 4 minutes. The boiling agarose was removed from the microwave oven to a water bath. It was stirred continuously to produce a uniform temperature and prevent setting of the gel on the walls of the glass beaker that were colder due to contact with the room temperature water. The gel was cooled to 60°C and was mixed with the solution in the other glass beaker which was at room temperature. No extra water was added to account for water loss by evaporation during boiling or cooling. No aeration, oxygenation or nitrogenation was applied to the gels. As the final volume of 250 ml of FAX gel was convenient for measurement and weighing of ingredients, all gel volumes were prepared in multiples of 250 ml. The mixed solution was stirred to produce a uniform solution and immediately poured into respective calibration vials or diffusion phantoms and placed in a refrigerator.

The second formulation of ferrous sulphate gel was FAX gel with additional sucrose. 500mg of the carbohydrate per 250ml of final gel volume was added to the glass beaker before agarose was added. Once the sucrose granules had dissolved the agarose powder was added.

The third formulation of ferrous sulphate gel was the traditional Fricke gel, referred to as FA gel in this communication. The method of preparation was the same as for the FAX gel but without either xylenol orange or carbohydrate additives.

Dose Response Measurements

Each gel formulation was prepared three times making a total of nine independent experiments. The gel was poured into a series of vials with screw-top lids and placed in a refrigerator. After each batch of gels had set the batch was irradiated to a known absorbed dose using a Co-60 Gammacell 200 (MDS Nordian, Canada) irradiation facility which had previously been calibrated[21]. Vials of gel were irradiated in intervals of 7 Gy up to 49 Gy.

For the purposes of imaging, vials were positioned in a purpose built container or 'phantom' (figure 1). The phantom consisted of a plastic container with a push-on lid. A plate was manufactured also from plastic to fit to the base inside the container to keep the vials positioned apart in the upright position during scanning. After the vials were placed in the container it was filled with tap water.

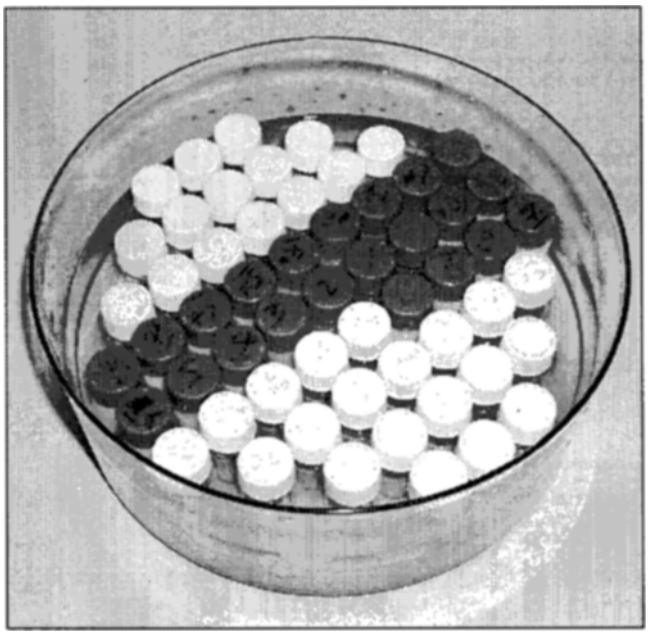

Figure 1. *Phantom container holding vials*

Magnetic resonance imaging (MRI) was undertaken using the head coil of a Siemens Vision (1.5 T) MRI scanner in order to determine the longitudinal or spin-lattice relaxation time, T_1 for each vial (figure 2). The phantom was imaged with a single slice in the coronal plane using a conventional spin-echo pulse sequence. An echo time (TE) of 12 ms and repeated repetition times (TR) with increasing values ranging from 25 ms up to 4000 ms were used. The field of view (FOV) was 110 x 110 mm, the slice thickness 5 mm and the pixel size 0.86 x 0.86 mm. One signal acquisition was used. Data were subsequently transferred to a personal computer and processed to calculate T_1 image 'maps' using software written in-house[22]. Having calculated the T_1 maps, regions of interest (ROI) of similar area of 0.54 cm^2 (57 pixels), were drawn on each vial to obtain T_1 values. T_1 and R_1 were then plotted against absorbed dose.

In order to calibrate T_1 measurements using this pulse sequence, a standard 1 litre stock solution of $^{153}GdCl^3$ of known relaxivity[23] in a volumetric flask was transferred to 50 ml volumetric flasks and further diluted to give solutions with a variety of relaxivities. The solution from each 50 ml flask was subsequently transferred to a series of vials. The vials were imaged and T_1 and T_2 for each was subsequently calculated. To ensure that images of the phantom in the head coil were acceptably uniform a similar series of vials containing solutions of the same T_1 were imaged and the standard deviation determined over the area of the phantom.

All scans were acquired at a temperature of 22° C which was the ambient temperature of the air conditioned scanning room.

Experiments were undertaken to determine the T_1 and R_1

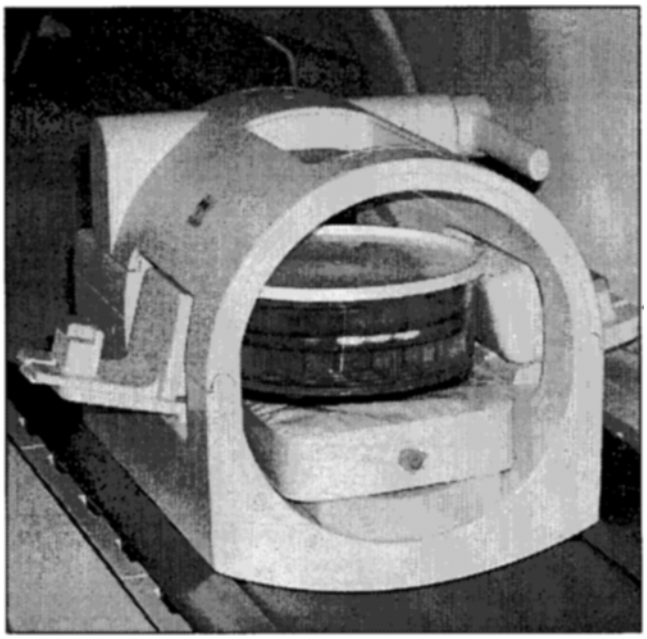

Figure 2. *Head coil of Siemens Vision MRI scanner containing phantom*

for each gel formulation in the irradiated range from 1 Gy up o 10 Gy in steps of 1 Gy.

Diffusion Measurements

For diffusion measurements, Perspex phantoms of 100 x 100 x 10 mm external dimensions and wall thickness 4 mm were constructed. Each gel formulation was poured into three phantoms. This enabled two diffusion measurements for each formulation to be undertaken whilst keeping the third phantom as a control.

One side of each phantom was open enabling the gel to be poured into the phantom. The gel set within a few minutes of pouring. A convex meniscus above the edge of the phantom was removed with a sharp scalpel blade. The side of the phantom was sealed with plastic adhesive tape to prevent dehydration and then placed in a refrigerator to reduce thermal oxidation.

The dose sensitivity curves obtained above were used to determine the dose required to obtain suitable contrast between irradiated and unirradiated regions of the phantom for the diffusion experiment. Two of the three phantoms for each gel formulation were irradiated to the required dose using a 6 MV linear accelerator (figure 3). Each phantom was placed on tissue substitute material to generate full backscatter. The phantom was irradiated using a square field of 4 cm measured at the surface of the phantom which had been positioned at 57 cm SSD. The third phantom was left unirradiated so as to act as a control sample (figure 4). After irradiation the phantoms were transported to the MRI scanning facility for imaging.

In order to reduce susceptibility effects during MRI measurements a section of perspex was added to the open side of each phantom, and held in place with plastic adhesive tape. The three phantoms were held together with plastic adhesive tape with the control sample in the centre. The three phantom assembly was then supported in the centre of the head coil with the faces of the phantoms parallel to the transverse plane of the scanner (figure 5).

The phantom assembly was scanned using the same spin-echo pulse sequence as that used for the dose sensitivity experiments. The parameters chosen for imaging were a TE of 12 ms and TR of 1000 ms. Three slices were chosen each with a thicknesses of 5 mm centred on each individual phantom.

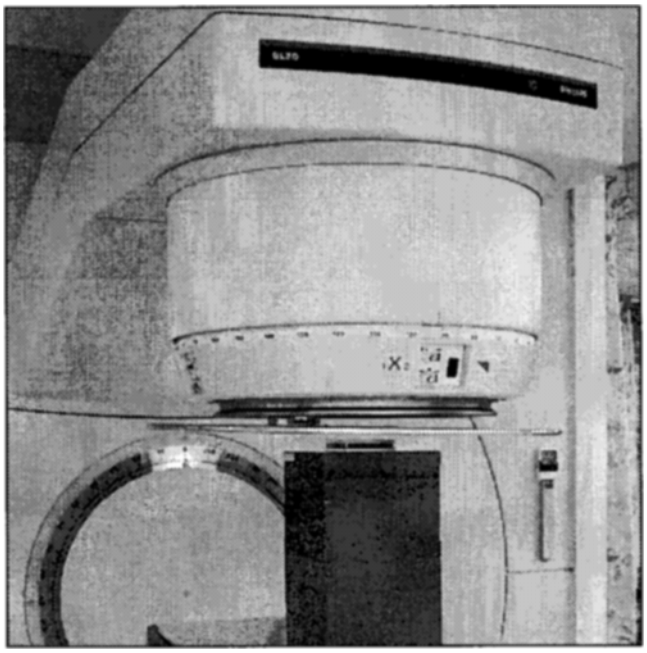

Figure 3. *Irradiation geometry of diffusion phantom using 6MV linear accelerator. Phantom irradiated at 57cm SSD.*

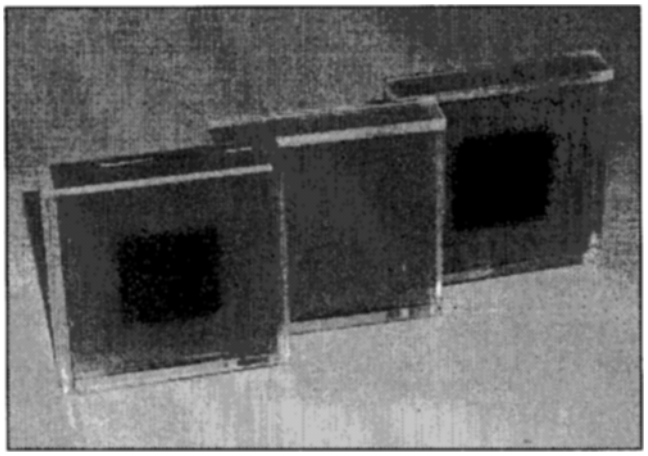

Figure 4. *Irradiated diffusion phantoms supported in head coil of MRI scanner*

The FOV was 110 x 110 mm and the pixel size 0.86 x 0.86 mm. Four signal averages were co-added. The acquisition time for each image was 9 minutes and 7 seconds.

The diffusion images were transferred to a personal computer for processing.

Mathematical Model

In this section we present a generic finite element method

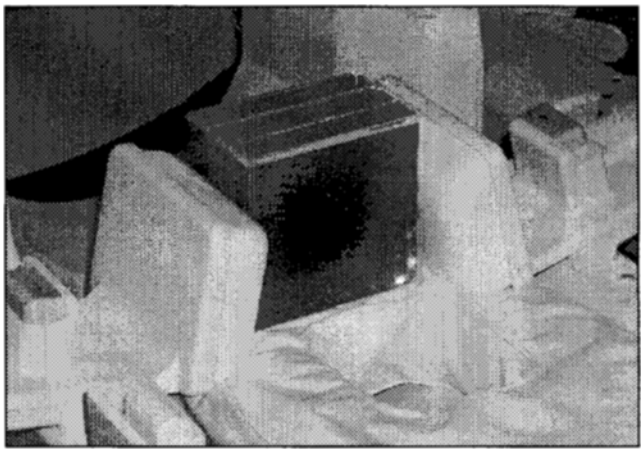

Figure 5. *Diffusion phantoms supported in head coil of MR scanner*

for determining the diffusion parameter from data obtained experimentally. In almost all of the previous work on this problem, including the previous work by the authors[11], concentration has been on solving problems where there is diffusion in only one space dimension. In this work, the method has been revised to consider diffusion problems in two space dimensions which more closely model what is happening in the vertically thin dosimetry gels that are being considered here.

The concentrations, u, of ferric (Fe^{3+}) ions in the gel were assumed to be modelled using a modified linear diffusion equation

$$\frac{\partial u}{\partial t} = \mu\left(\frac{\partial^2 u}{\partial x^2} + \frac{\partial^2 u}{\partial y^2}\right) + a \qquad (1)$$

where μ is the diffusion coefficient and is a parameter, which we will refer to as the drift parameter, which accounts for any drift in the signal intensities due to effects such as thermal oxidation. Thus in the absence of any diffusion ($\mu = 0$) this equation would model changes in the concentrations due to any oxidation of the gel, whilst if no drift ($a = 0$) was present equation (1) would model the purely diffusive processes in the gel. Because there is no flow of ions across the edges of the gel the concentrations cannot vary across the boundary, leading to the boundary condition.

$$\frac{\partial u}{\partial n} = 0. \qquad (2)$$

Let R denote the region occupied by the gel and let C denote the closed boundary of R. Given that the concentrations for time at all points in are known (the initial condition) and that suitable boundary conditions on C are specified for all time, it should be possible to solve equation (1) to predict the concentrations at some later time. However, analytical solutions of equation (1) for arbitrary initial and boundary conditions can usually only be expressed in terms of slowly converging infinite series whose coefficients may be difficult to calculate. Further, since the initial condition is not given as a continuous function but as point-wise values located at the pixels of the computer image, it is simpler to use approximate methods, such as the finite element method or the finite difference method, to solve equation.

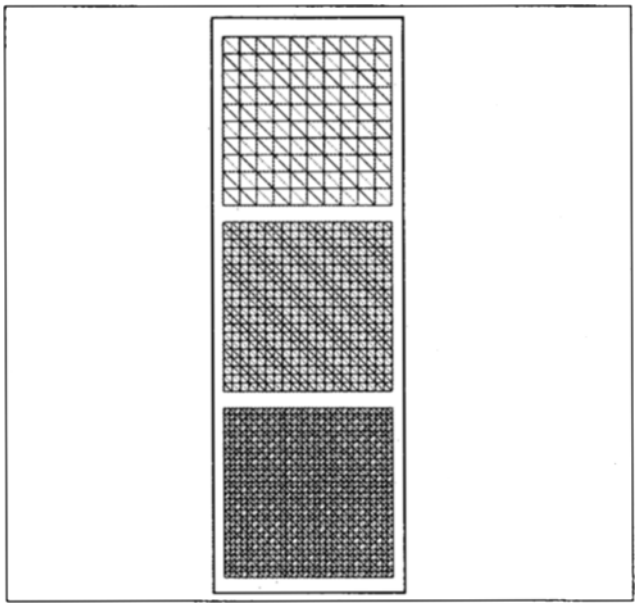

Figure 6. *Three meshes of 121,441 and 961 nodes*

Here the chosen solution method is the finite element method. Although the initial formulation of the finite element method is more complicated than that for the finite difference method, the finite element method can readily accommodate difficult domains, such as those with curved boundaries, without any further analysis, whereas the finite difference method cannot deal with such situations without a lot of further analysis.

The domain, R of the differential equation is divided into m simple elements, such as the triangles used here, at n node points. The nodes and elements are collectively referred to as the finite element mesh. Typical meshes are shown in figure 6. The location of the nodes should coincide with the locations of the pixels in the underlying computer image as the nodes are the points at which the approximate solution to the differential equation will be computed.

The concentration is approximated by

$$\tilde{u} = \sum_{j=1}^{n} u_j(t)\phi_j(x,y) \qquad (3)$$

where $u_j(t), j=1,\ldots,n$ are a set of time-dependent coefficients to be determined and $\phi_j(x,y), j=1,\ldots,n$ are a set of pre-determined linearly independent basis functions. Note that for simplicity the dependence of the basis functions on the space variables $(x,y)$and the dependence of the coefficients on time t will not be explicitly stated from now on. Although it is possible to choose any set of linearly independent functions to be used as the basis functions, they are usually chosen such that the j'th basis function is equal to one at the j'th node and equal to zero at all the other nodes. Thus u_j becomes a direct approximation to u at the j'th node. Further, the 'th basis function is usually chosen to be low-order polynomial (such as the linear functions used here) in any element which has node as one of its nodes and zero over all other elements. This choice of basis

functions yields an approximate solution which is continuous over R, but which does not have continuous derivatives at the element boundaries. Further, this choice of basis function reduces the amount of computational work that is required as in any given element there will only be three basis functions which are non-zero. More details on the choice of basis functions can be found in one of the many texts on the subject of finite elements, such as[24-26] for example.

Replacing u by μ in the differential equation (1) will yield a residual $r(x,y,t)$ as, in general, μ will not be the exact solution of the differential equation. That is,

$$\frac{\partial \tilde{u}}{\partial t} = \mu\left(\frac{\partial^2 \tilde{u}}{\partial x^2} + \frac{\partial^2 \tilde{u}}{\partial y^2}\right) + a + r(x,y,t). \qquad (4)$$

The Galerkin finite element method requires that the coefficients u_j are chosen such that the residual is orthogonal to each of the basis functions for all time. That is, the coefficients are chosen such that

$$\iint_R r\phi_i \, dx\,dy = 0 \qquad i = 1,2,\ldots,n \qquad t \geq 0. \qquad (5)$$

This leads to

$$\iint_R \frac{\partial \tilde{u}}{\partial t}\phi_i \, dx\,dy = \mu\iint_R\left(\frac{\partial^2 \tilde{u}}{\partial x^2} + \frac{\partial^2 \tilde{u}}{\partial y^2}\right)\phi_i \, dx\,dy + a\iint_R \phi_i \, dx\,dy. \qquad (6)$$

An application of Green's theorem[24] to the first integral on the right-hand side of equation (6) and replacing u by equation (3) gives

$$\sum_{j=1}^{n}\frac{du_j}{dt}\iint_R \phi_j\phi_i \, dx\,dy = \mu\left[\sum_{j=1}^{n} u_j \iint_R -\frac{\partial\phi_i}{\partial x}\frac{\partial\phi_j}{\partial x} - \frac{\partial\phi_i}{\partial y}\frac{\partial\phi_j}{\partial y}\,dx\,dy\right] + \mu\oint_C \frac{\partial \tilde{u}}{\partial n}\phi_i \, dC + a\iint_R \phi_i \, dx\,dy. \qquad (7)$$

Since the approximate solution is assumed to satisfy any Neumann (derivative) boundary conditions exactly, and in the problem considered here the boundary conditions are

$$\frac{\partial u}{\partial n} = 0. \qquad (8)$$

on the whole of the boundary, the line integral on the right-hand side of equation (7) will be zero. Thus equation (7) can be written in matrix notation as

$$M\dot{\mathbf{u}} = \mu K\mathbf{u} + a\mathbf{f} \qquad (9)$$

where

$$M_{ij} = \iint_R \phi_i\phi_j \, dx\,dy \qquad (10)$$

$$K_{ij} = \iint_R\left(-\frac{\partial\phi_i}{\partial x}\frac{\partial\phi_j}{\partial x} - \frac{\partial\phi_i}{\partial y}\frac{\partial\phi_j}{\partial y}\right)dx\,dy \qquad (11)$$

$$\mathbf{f}_i = \iint_R \phi_i \, dx\,dy \qquad (12)$$

and $\mathbf{u} = [u_1, u_2, \mathbf{K}, u_n]^T$ and $\dot{\mathbf{u}} = \left[\frac{du_1}{dt}, \frac{du_2}{dt}, \ldots, \frac{du_n}{dt}\right]^T$. In an analogy with the finite element method for structural motion problems, the matrix K is called the stiffness matrix, the matrix M is called the mass matrix and the vector $\mathbf{f}$ is called the load vector.

Equation (9) can now be viewed as a coupled system of linear first order ordinary differential equations, and solved using the appropriate techniques for such systems. It can be shown that the matrix M is always non-singular provided that the basis functions are linearly independent and so

$$\begin{aligned}\dot{\mathbf{u}} &= \mu M^{-1}K\mathbf{u} + aM^{-1}\mathbf{f} \\ &= \mu A\mathbf{u} + aM^{-1}\mathbf{f}\end{aligned} \qquad (13)$$

where $A = M^{-1}K$. From linear algebra, it is well known that[27]

$$A = PDP^{-1} \qquad (14)$$

where D is a diagonal matrix with $D_{ii} = \lambda_i$ where λ_i is an eigenvalue A of and the i'th column of P is the corresponding eigenvector. Thus equation (13) becomes

$$P^{-1}\dot{\mathbf{u}} = \mu DP^{-1}\mathbf{u} + aP^{-1}M^{-1}\mathbf{f} \qquad (15)$$

Making the change of variables $\mathbf{u} = P\mathbf{w}$ leads to

$$\dot{\mathbf{w}} = \mu D\mathbf{w} + a\mathbf{g} \qquad (16)$$

where $\mathbf{g} = P^{-1}M^{-1}\mathbf{f}$. The i'th equation of the system of equations in (16) is

$$\dot{w}_i = \mu\lambda_i w_i + a g_i \qquad i = 1,2,\ldots,n \qquad (17)$$

which has solution

$$w_i = \begin{cases} e^{\mu\lambda_i t}w_{i0} + ag_i\dfrac{e^{\mu\lambda_i t}-1}{\mu\lambda_i} & \lambda_i \neq 0 \\ w_{i0} + agt & \lambda_i = 0 \end{cases} \qquad (18)$$

where W_{i0} is the value of W_i when $t = 0$. Hence the solution to equation (16) can be written in the form

$$\mathbf{w}(t) = E(\mu,t)\mathbf{w}(0) + aF(\mu,t)\mathbf{g} \qquad (19)$$

where E and F are diagonal matrices with elements

$$E_{ii} = e^{\mu\lambda_i t}$$

$$F_{ii} = \begin{cases} \dfrac{e^{\mu\lambda_i t}-1}{\mu\lambda_i} & \lambda_i \neq 0 \\ t & \lambda_i = 0. \end{cases} \qquad (20)$$

Reversing the change of variables gives the solution to the original equations as

$$\mathbf{u}(t,\mu,a) = PE(\mu,t)P^{-1}\mathbf{u}(0) + aPF(\mu,t)P^{-1}M^{-1}\mathbf{f}. \qquad (21)$$

Thus given the concentrations at time $t = 0$ it is possible to calculate the concentrations at any later time using equation (21). It is noted at this point that the matrices P and M

appearing in equation (21) depend only on the geometry of the finite element mesh, and so only need to be computed once for any given mesh. Further, the eigenvalues which appear in the definitions of the matrices E and F only need to be computed once for any given mesh, and so once these have been found the solution can be computed relatively quickly for different values of the parameters μ and a and for different end times t.

Using equation (21) it is possible to construct a method for estimating the values of the diffusion coefficient μ and drift parameter a from experimental data. Let $\mathbf{v}(0)$ and $\mathbf{v}(0)$ denote vectors of the nodal values of the initial and final concentrations respectively which have been obtained from experimental data. Now, for given values of μ and a it is possible to compute $\mathbf{u}(t,\mu,a)$ using equation (21) with $\mathbf{u}(0) = \mathbf{v}(0)$. If

$$S = \sum_{i=1}^{n} \left(u_i(t,\mu,a) - v_i(t)\right)^2 \qquad (22)$$

then the required values of μ and a are those which minimise S. There are a number of methods for minimising functions of the form of equation (22), and the method employed here is the method of steepest descent. Given some starting point (μ_0, a_0) a new point (μ_1, a_1) is found which minimises in the direction of steepest descent at (μ_0, a_0). It can be shown (Fletcher, 1980) that

$$\mu_1 = \mu_0 - h\frac{\partial S}{\partial \mu}(\mu_0,a_0) \qquad a_1 = a_0 - h\frac{\partial S}{\partial a}(\mu_0,a_0) \qquad (23)$$

where h is the distance to proceed in the direction of steepest descent. A good estimate of h can be found by using a single step one-dimensional Newton method to minimise S with respect to h. After some analysis it is possible to show that

$$h = \frac{\left[\left(\frac{\partial S}{\partial \mu}\right)^2 + \left(\frac{\partial S}{\partial a}\right)^2\right]}{\frac{\partial^2 S}{\partial \mu^2}\left(\frac{\partial S}{\partial \mu}\right)^2 + 2\frac{\partial^2 S}{\partial \mu \partial a}\frac{\partial S}{\partial \mu}\frac{\partial S}{\partial a} + \frac{\partial^2 S}{\partial a^2}\left(\frac{\partial S}{\partial a}\right)^2} \qquad (24)$$

where all of the derivatives appearing in equation (24) are evaluated at the point (μ_0, a_0). Although it is possible to use more Newton iterations to obtain a better estimate h of it is more efficient to simply employ a single iteration and find the direction of steepest descent at the new point and proceed in the new direction. It should be noted that it is possible to analytically differentiate equation (22) to obtain expressions for all the derivatives appearing in equation (23) and equation (24), and these are given in Appendix A.

Test Problem

In order to demonstrate that the above method could be used to estimate the diffusion and drift parameters, the model was applied to the following test problem.

It is relatively simple to show that

$$u(x,y,t) = \frac{u_0}{2}\left[\exp\left(-\frac{2\mu\pi^2 t}{L^2}\right)\cos\left(\frac{\pi x}{L}\right)\cos\left(\frac{\pi y}{L}\right) + 1\right] + at \qquad (25)$$

(where u_0 is a parameter that controls the magnitude of the initial solution) is a solution to equation (1) on the square $0 \le x,y \le L$ and satisfies the boundary condition

$$\frac{\partial u}{\partial n} = 0. \qquad (26)$$

around the whole of the boundary. The test problem was generated by forming a mesh on the square and then choosing values for μ and a so that the exact solution could be computed at the nodes using equation (25). Then random errors were introduced into the data to simulate the effect of the experimental errors in the data. The finite element model was then used to estimate the values of μ and a from data with the random errors and these values were compared with the exact values.

Figure 7 shows the mean relative error in the calculated value of the diffusion coefficient μ for the test problem for different elapsed times, where the process of generating random errors in the data has been repeated 100 times. The test was performed three times with the maximum error in the concentration at any one node set to be 2.5%, 5% and 10% of u_0. The corresponding results for the drift parameter a are shown in Figure 8. The results presented here are for a square with L=10 using a mesh with 961 nodes (a 31 x 31 grid of nodes) and the exact values of the parameters are μ=0.9 and a=10.

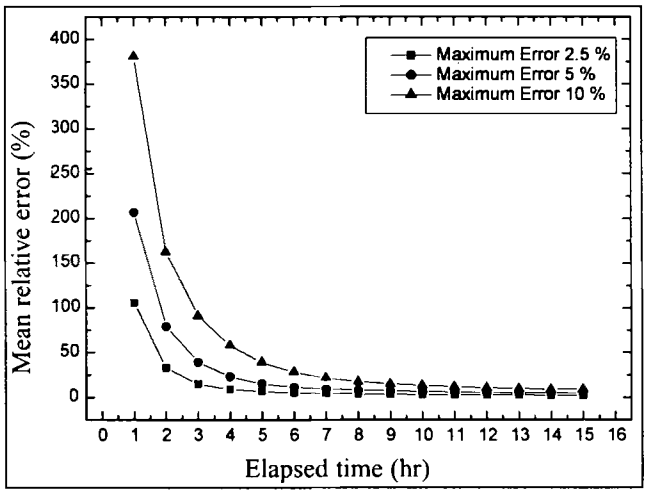

Figure 7. *Mean relative error in the fitted diffusion coefficient for the test problem using different magnitude random errors in the original data.*

It can be seen from figures 7 and 8 that the error in the fitted parameters is less when the errors in the underlying data are smaller. Further, the graphs show that the accuracy of the estimates improves as the elapsed time increases. These results illustrate that the method can be used to determine the diffusion coefficient and drift parameters to a reasonable degree of accuracy using the method proposed in this paper.

Results

Figure 9 shows the variation in measured T_1 with nominal T_1

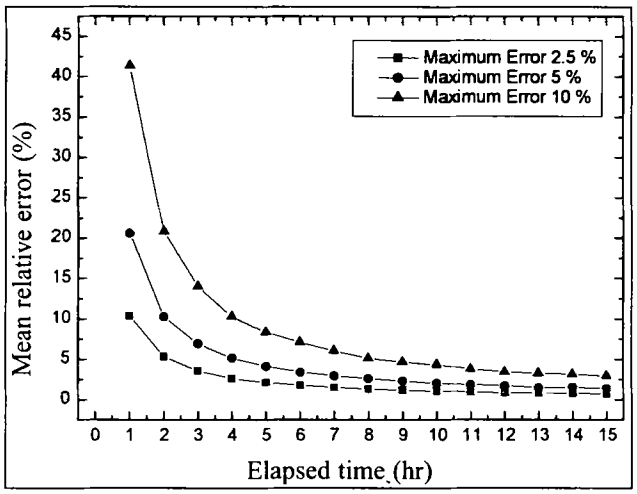

Figure 8. *Mean relative error in the fitted drift parameter for the test problem using different magnitude random errors in the original data.*

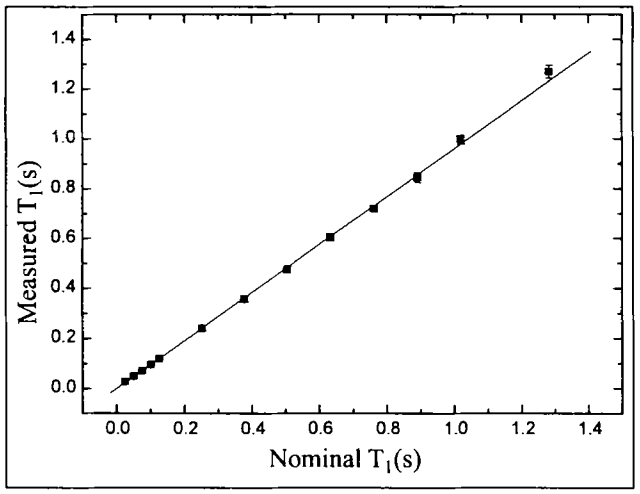

Figure 9. *Measured T_1 vs nominal T_1 for Gd solutions*

for the vials of $GdCl_3$ solution. The error bars are calculated as the standard deviation in the pixel values in the ROI.

The regression gave an r^2 of 0.9995, $p < 10^{-17}$ and standard error of regression of 0.00789. The calculated slope of 0.9603 from the regression indicated the measured T_1 was in reasonable agreement with the nominal value of T_1.

Figure 10 shows the variation of R_1 with radiation dose up to 49 Gy. It should be noted that each data point is a mean from three separate experiments. Figure 11 shows repeat experiments for the three gel formulations that were irradiated at 1 Gy intervals up to 10 Gy. A dose sensitivity of 12.5, 34.8 and 82.8 $s^{-1}kGy^{-1}$ for FAX, FAX / sucrose and FA gels respectively were calculated from figure 11.

Figure 12 illustrates the variation in signal intensity in the spin echo images of figure 10 with a TE of 12.5 ms and TR of 1000 ms.

Figure 13 illustrates a time series of diffusion images from one of the phantoms. Each signal intensity image was acquired with a TE of 12.5 ms and TR of 1000 ms at intervals of 30 minutes.

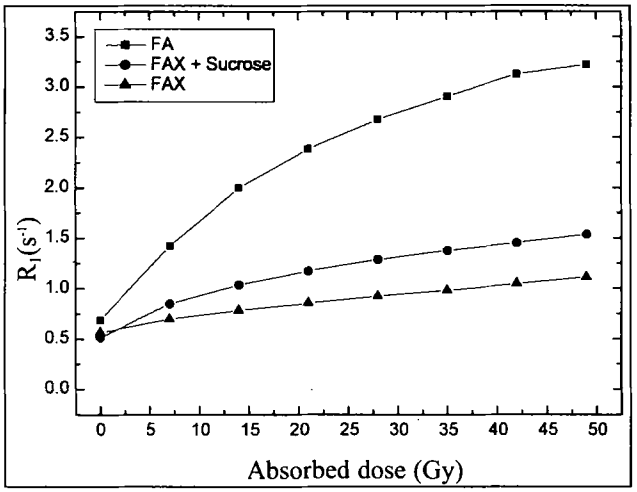

Figure 10. *Longitudinal relaxation rate vs absorbed radiation dose*

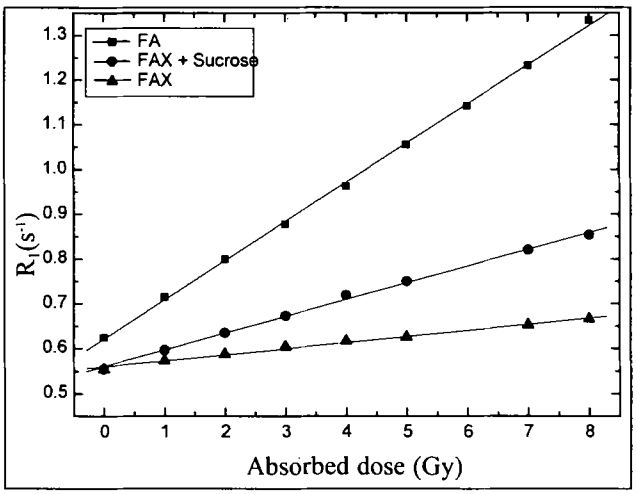

Figure 11. *Longitudinal relaxation rate vs absorbed radiation dose*

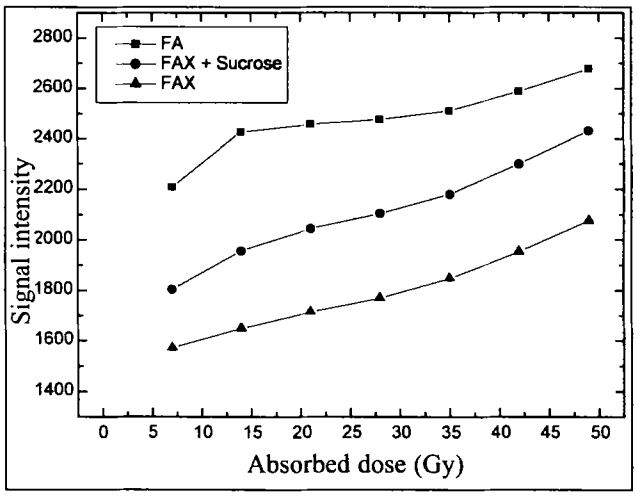

Figure 12. *Signal intensity vs absorbed dose*

Figure 14 shows a plot of the diffusion coefficients determined for one of the phantoms of FAX gel. Each plot also indicates the effect on the measurement of choice of mesh size of 121, 441 and 961 nodes in the calculation. Each data point

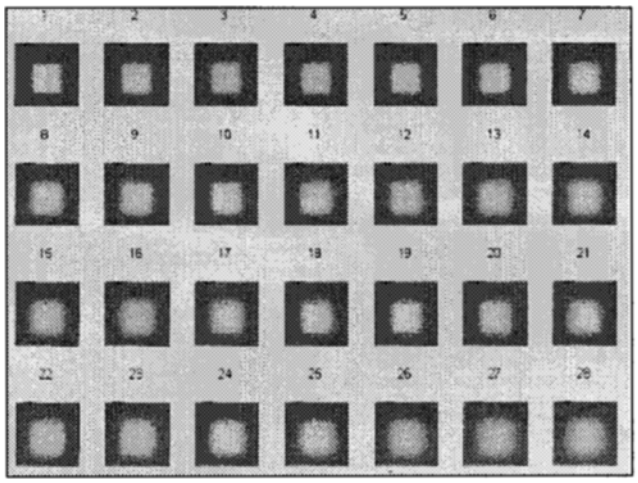

Figure 13. *Signal intensity images acquired at 30 minute intervals with a TE of 12.5ms and TR of 1000ms*

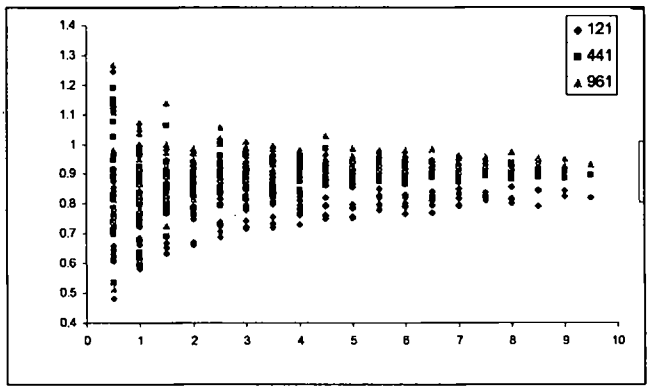

Figure 14. *Fitted diffusion coefficients for the FAX gel.*

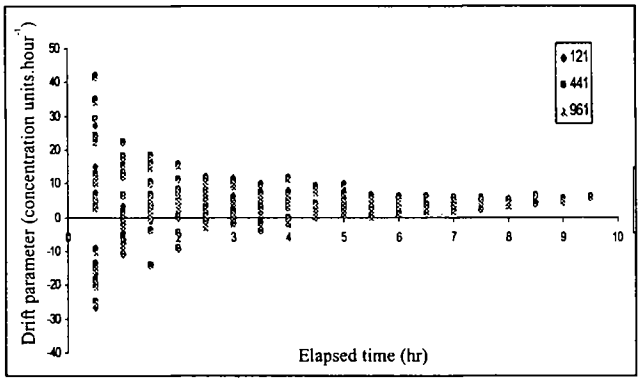

Figure 15. *Fitted values of the drift parameter for the FAX gel.*

corresponds to the diffusion coefficient calculated between two specific time periods. It is clear from Figure 14 that the variation in calculated diffusion coefficient decreases as the elapsed time increases.

Figure 15 presents the drift parameter for the FAX gel formulation for each mesh.

Table 2 gives a summary of the results of the calculated diffusion coefficient for each gel formulation. Each value quoted is the mean of the values obtained for elapsed times longer than six hours, and for both gel samples for each formulation. The quoted error level gives the 95% confidence interval for the fitted parameter. The corresponding results for the drift parameter are given in Table 3.

The values for the drift parameter evaluated by this method in Table 3 have large uncertainties. However, these must be considered in relation to the magnitude of the original concentrations. In the present case, the drift parameters correspond to approximately 0.1% per hour. Drift is therefore negligible and the large uncertainties in its evaluation not unexpected.

Number of Nodes	FA Gel (10^{-3} cm^{2}h^{-1})	FAX + XO Gel (10^{-3} cm^{2}h^{-1})	FAX + XO + Sucrose Gel (10^{-3} cm^{2}h^{-1})
121	10.3±1.1	8.6±0.6	7.9±0.6
441	12.5±0.7	9.2±0.3	8.7±0.7
961	13.3±0.6	9.7±0.4	9.5±0.8

Table 2. *Summary of results for the diffusion coefficient.*

Discussion and Conclusions

The non-linearity of the dose sensitivity curves up to 49 Gy is likely to be due to the aqueous gel solutions not being oxygenated by bubbling oxygen through them during manufacture. This phenomenon has been investigated by other researchers[5]. Although the gel formulations could have been optimised further by bubbling oxygen or modification of the chemical constituents it is considered that the formulations used would be adequate as the primary aim of this work was to investigate diffusion. The dose sensitivities of 12.5, 34.8 and 82.8 s^{-1} kGy^{-1} for FAX, FAX / sucrose and FA gels respectively for the dose range 0-9 Gy correspond favourably with values quoted in the literature for gels of similar composition[13].

The temperature of the phantoms was kept constant throughout the experiment. Therefore, thermal effects which may have contributed to a non-constant diffusion coefficient were assumed to be minimal and were ignored.

The control phantom positioned between the two outer diffusion phantoms was used to investigate non-uniformities in the imaging.

Figure 16 is a profile plotted across one of the images acquired from the control phantom illustrating a systemati non-uniformity. However, the magnitude of this non-uniformity is small compared to the magnitude of the concentrations being measured, and of the same order of magnitude as the random variations in the data. Hence it is likely that the error induced by this non-uniformity is negligible compared to the other errors in the calculation.

In order to estimate the uncertainty in the signal intensity in any pixel, the variation in individual pixel intensities throughout the time series of images was investigated. Nine individual central pixels were selected. The standard deviation (SD) in signal intensity was calculated for each of these pixels through the set of control images giving a total of nine SD's with a mean SD of 3.9 %. This value was compared with the results of the test problem to provide an estimate of the overall uncertainty in the diffusion coefficient (Table 2).

Number of Nodes	FA Gel (signal intensity h-1)	FAX + XO Gel (signal intensity h-1)	FAX + XO + Sucrose Gel (signal intensity h-1)
121	-1.5+5.2	4.0+3.2	-1.9+7.0
441	-1.5+5.3	3.8+3.1	-1.9+7.2
961	-1.4+5.2	3.6+3.1	-2.0+7.2

Table 3. *Summary of results for the drift parameter.*

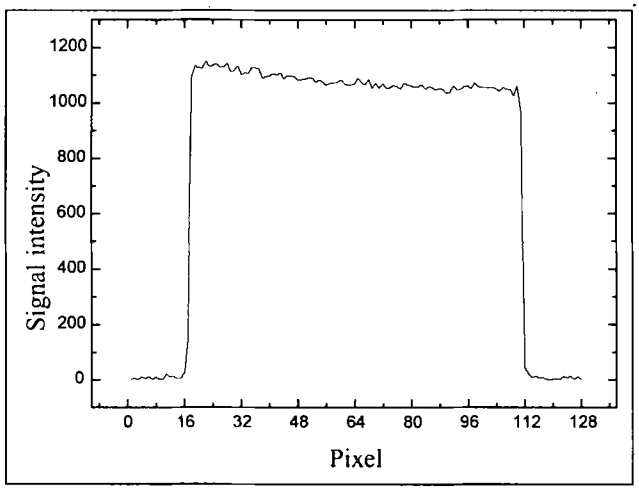

Figure 16. *Profile across control phantom image illustrating non-uniformity.*

There is clearly a systematic dependence of the value obtained for the diffusion coefficient, μ on the number of nodes used in the finite element mesh (see Table 2) so that averaging the values obtained for the different mesh sizes is not appropriate. We believe that this systematic variation arises from the dependence, on mesh size, of the effective concentration gradients in the digitised initial distributions, particularly across the edges of the irradiated areas of the phantoms. Since the largest number of nodes provides the closest approximation to the true gradients, we believe that the 961 node results provide the best estimate of the diffusion coefficient.

T_1-weighted spin echo images provides a qualitative description of the ferric ion distribution in dosimetry gels[28]. Variations between signal intensity and relaxation rate are dependent on the imaging parameters, TE and TR and the sensitivity ($s^{-1}Gy^{-1}$)[14]. Errors may be encountered due to using signal intensities from diffusion images rather than calculated R_1 values. However, these were simulated to be as low as 2 % but in some unfavourable situations as high as 70 %. To reduce errors a reduction in TE, TR and sensitivity would be required. Errors in diffusion calculations as low as 2% were found in work utilising T_1-weighted spin echo images[12].

The magnitude of the diffusion coefficient determined in this work is considered to be too large to make the gels clinically useful in radiotherapy dosimetry applications and this has motivated the development of alternative polymer dosimetry gels[29-32]. However, as polymer gel dosimeters rely on free-radical chemistry with the associated problems of oxygen 'contamination' and due to the toxic nature of the chemicals used it would be desirable to solve the diffusion problem in FAX. This might be achieved by either reducing the diffusion further by chemical means or alternatively using the finite element method to solve the diffusion equation for negative times. This latter approach would enable the dose distribution at the time of irradiation to be determined from that measured at a later time.

In theory, the mathematical model presented here could be used to solve the diffusion problem for a negative time by simply specifying a negative time in equation (21), and this would yield the correct result if infinite precision arithmetic was used in all the calculations. However, it is well known that this is an unstable problem in the sense that any small changes in the initial data can produce errors in the final result which are the same size or larger than the quantity that we are interested in. Since the computer has to round all internal values to a known but finite precision, the effects of these rounding errors will dominate the calculation even for very small negative times. This effect actually gets worse as the number of finite element nodes increases as the errors in the final solution are essentially related to magnitude of the largest eigenvalue which will increase as the number of nodes increases.

Acknowledgments

Useful discussions with S Keevil, J Pope, T Kron and B Shuter are acknowledged. The support of Southern X-ray Clinics and the Wesley Research Institute, Wesley Hospital, Brisbane and the Queensland Cancer Fund are acknowledged. Data processing by P Murry is acknowledged.

APPENDIX A.

The following expressions give the derivatives of the function S given by equation (20) which has to be minimised. Recall

$$S = \sum_{i=1}^{n} \left(u_i(t,\mu,a) - v_i(t)\right)^2$$

Let $\mathbf{w} = P^{-1}\mathbf{u}(0)$, $\mathbf{g} = P^{-1}M^{-1}\mathbf{f}$ and form the six summations $s_{1i},\ldots,s_{6i}$

$$s_{1i} = \sum_{j=1}^{n} P_{ij} E_{jj}(\mu,t) w_j$$

$$s_{2i} = \sum_{j=1}^{n} P_{ij} F_{jj}(\mu,t) g_j$$

$$s_{3i} = \sum_{j=1}^{n} P_{ij} \frac{\partial E_{jj}(\mu,t)}{\partial \mu} w_j$$

$$s_{4i} = \sum_{j=1}^{n} P_{ij} \frac{\partial F_{jj}(\mu,t)}{\partial \mu} g_j$$

$$s_{5i} = \sum_{j=1}^{n} P_{ij} \frac{\partial^2 E_{jj}(\mu,t)}{\partial \mu^2} w_j$$

$$s_{6i} = \sum_{j=1}^{n} P_{ij} \frac{\partial^2 F_{jj}(\mu,t)}{\partial \mu^2} g_j$$

Then

$$S = \sum_{i=1}^{n} (s_{1i} + a s_{2i} - v_i(t))^2$$

$$\frac{\partial S}{\partial \mu} = -2\sum_{i=1}^{n} [(v_i(t) - s_{1i} - a s_{2i})(s_{3i} + a s_{4i})]$$

$$\frac{\partial^2 S}{\partial \mu^2} = 2\sum_{i=1}^{n} [(-s_{3i} - a s_{4i})^2 + (v_i(t) - s_{1i} - a s_{2i})(-s_{5i} - a s_{6i})]$$

$$\frac{\partial S}{\partial a} = -2\sum_{i=1}^{n} [(v_i(t) - s_{1i} - a s_{2i}) s_{2i}]$$

$$\frac{\partial^2 S}{\partial a^2} = 2\sum_{i=1}^{n} (s_{2i})^2$$

$$\frac{\partial^2 S}{\partial \mu \, \partial a} = -2\sum_{i=1}^{n} [(-s_{3i} - a s_{4i}) s_{2i} + (v_i(t) - s_{1i} - a s_{2i}) s_{4i}]$$

References

1. Day, M.J. and Stein, G., *Chemical effects of ionizing radiation in some gels*, Nature. 166: 146-7, 1950.
2. Andrews, H.L., Murphy, R.E., and LeBrun, E.J., *Gel dosimeter for depth dose measurements*, The Review of Scientific Instruments. 28: 329-32, 1957.
3. Gore, J.C., Kang, Y.S., and Schulz, R.J., *Measurement of radiation dose distributions by nuclear magnetic resonance (NMR) imaging*, Phys. Med. Biol. 29: 1189-97, 1984.
4. Fricke, H. and Morse, S., *The chemical action of roentgen rays on dilute ferrous sulfate solutions as a measure of radiation dose*, Am. J. Roentgenol. Radium Therapy Nucl. Med. 18: 430-2, 1927.
5. Schulz, R.J., deGuzman, A.F., Nguyen, D.B., and Gore, J.C., *Dose-response curves for Fricke-infused agarose gels as obtained by nuclear magnetic resonance*, Phys. Med. Biol. 35: 1611-22, 1990.
6. Olsson, L.E., Westrin, B.A., Fransson, A., and Nordell, B., *Diffusion of ferric ions in agarose dosimeter gels*, Phys. Med. Biol. 37: 2243-52, 1992.
7. Balcom, B.J., Lees, T.J., and Sharp, A.R., *Diffusion of Fe(III) in agarose radiation dosimetry phantoms*, Proceedings of Society of Magnetic Resonance in Medicine, 1994.
8. Balcom, B.J., Lees, T.J., Sharp, A.R., Kulkarni, N.S., and Wagner, G.S., *Diffusion in Fe(II/III) radiation dosimetry gels measured by magnetic resonance imaging*, Phys. Med. Biol. 40: 1665-76, 1995.
9. Baldock, C., Harris, P.J., Piercy, A., Patval, S., Prior, D.N., Keevil, S.F., and Summers, P., *Temperature dependance of diffusion in Fricke gel MRI dosimetry*, Med. Phys. 22: 1540, 1995.
10. Baldock, C., Harris, P.J., Piercy, A., Patval, S., Prior, D.N., Keevil, S.F., and Summers, P., *Investigation of temperature dependance of diffusion in agar Fricke gel for MRI dosimetry*, Proceedings of International Society for Magnetic Resonance in Medicine. 22: 1540, 1995.
11. Harris, P.J., Piercy, A., and Baldock, C., *A method for determining the diffusion coefficient in Fe(II/III) radiation dosimetry gels using finite elements*, Phys. Med. Biol. 41: 1745-53, 1996.
12. Rae, W.I.D., Willemse, C.A., Lotter, M.G., Engelbrecht, J.S., and Swarts, J.C., *Chelator effect on ion diffusion in ferrous-sulfate-doped gelatin gel dosimeters as analyzed by MRI*, Med. Phys. 23: 15-23, 1996.
13. Kron, T., Jonas, D., and Pope, J.M., *Fast T-1 imaging of dual gel samples for diffusion measurements in NMR dosimetry gels*, Magn. Reson. Imaging. 15: 211-21, 1997.
14. Pedersen, T.V., Olsen, D.R., and Skretting, A., *Measurement of the ferric diffusion coefficient in agarose and gelatine gels by utilization of the evolution of a radiation induced edge as reflected in relaxation rate images*, Phys. Med. Biol. 42: 1575-85, 1997.
15. Schreiner, L.J., Crooks, I., Evans, M.D.C., Keller, B.M., and Parker, W.A., *Imaging of HDR brachytherapy dose distributions using NMR Fricke-gelatin dosimetry*, Magn. Reson. Imaging. 12: 901-7, 1994.
16. Chu, W.C., Kao, Y.H., Chung, W.Y., Guo, W.Y., and Pan, H.C., *Ferric ion diffusion effects in NMR-Fricke-agarose dosimetry*, Proceedings of International Society for Magnetic Resonance in Medicine, 1998.
17. Chu, K.C., Jordan, K.J., Battista, J.J., Van Dyk, J., and Rutt, B.K., *Polyvinyl alcohol-Fricke hydrogel and cryogel: two new gel dosimetry systems with low Fe3+ diffusion*, Phys. Med. Biol. 45: 955-69, 2000.
18. Clarke, G.D., McColl, R.W., Maryanski, M.J., and Glatstein, E., *Imaging of radiation dose in two different types of gel-based dosimeters: a comparison between FAX and BANG*, Med. Phys. 22: 951, 1995.
19. Olsson, L.E., *PhD*, Thesis, Lund University, Malmo, 1991.
20. Zahmatkesh, M., *PhD*, Thesis, Queensland University of Technology, Brisbane, 1999.
21. Baldock, C., Fitchew, R., Murry, P.J., Murry, M., Back, P., and Kron, T., *Calibration of Gammacell irradiator for irradiation of radiotherapy polymer dosimetry gel*, Med. Phys. 26: 1130, 1999.
22. Murry, P. and Baldock, C., *Research software for MRI radiotherapy gel dosimetry*, Australasian Physical & Engineering Sciences in Medicine. 23: 44-51, 2000.
23. Shuter, B., *PhD*, Thesis, University of New South Wales, Sydney, 1999.
24. Davies, A.J., *The finite element method*, Oxford University Press, Oxford, 1980.
25. Bickford, W.B., *A first course in the finite element method*, Richard D. Irwin Inc, Boston, 1994.
26. Zienkiewicz, O.C. and Taylor, R.L., *The finite element method, vols 1 and 2*, McGraw Hill, London, 1989.
27. Fox, L., *An introduction to numerical linear algebra*, Oxford University Press, Oxford, 1964.
28. Prasad, P.V., Nalcioglu, O., and Rabbani, B., *Measurement of three-dimensional radiation dose distributions using MRI*, Radiation Research. 128: 1-13, 1991.
29. Maryanski, M.J., Gore, J.C., Kennan, R.P., and Schulz,

R.J., *NMR relaxation enhancement in gels polymerized and cross-linked by ionizing radiation: a new approach to 3D dosimetry by MRI*, Magn. Reson. Imaging. 11: 253-8, 1993.

30. Maryanski, M.J., Schulz, R.J., Ibbott, G.S., Gatenby, J.C., Xie, J., Horton, D., and Gore, J.C., *Magnetic resonance imaging of radiation dose distributions using a polymer-gel dosimeter*, Phys. Med. Biol. 39: 1437-55, 1994.
31. Maryanski, M.J., Ibbott, G.S., Schulz, R.J., Xie, J., and Gore, J.C., *Magnetic resonance imaging of radiation dose distributions in tissue-equivalent polymer-gel dosimeters, Proceedings of Society of Magnetic Resonance in Medicine*, 1994.
32. Baldock, C., Burford, R.P., Billingham, N., Wagner, G.S., Patval, S., Badawi, R.D., and Keevil, S.F., *Experimental procedure for the manufacture and calibration of polyacrylamide gel (PAG) for magnetic resonance imaging (MRI) radiation dosimetry*, Phys. Med. Biol. 43: 695-702, 1998.